EXACT COHERENT STRUCTURES IN SPATIOTEMPORAL CHAOS: FROM QUALITATIVE DESCRIPTION TO QUANTITATIVE PREDICTIONS

A Thesis Proposal
Presented to
The Academic Faculty

by

Nazmi Burak Budanur

In Partial Fulfillment
of the Requirements for the Degree
Doctor of Philosophy in the
School of Physics

Georgia Institute of Technology

TABLE OF CONTENTS

CHAPTER I

INTRODUCTION

Irregular patterns in space and time arise in various physical settings, where dynamics are determined by nonlinear partial differential equations (PDEs). The examples range from cardiac dynamics to chemical reactions and fluid mechanics. While most of these equations are numerically solvable with high accuracy, theoretical understanding of their dynamics is far from being complete. The reasons of this incompleteness can be classified into two categories: technical difficulties and gaps in theory. Even though the theory of nonlinear dynamics is well established, applications of its methods, even the simplest ones, to PDEs can be highly non-trivial due to the fact that PDEs are infinite dimensional systems. In addition to technical difficulties, one also encounters theoretical problems that were never addressed or fully resolved. The main problem to be addressed in the proposed thesis, namely the continuous symmetry reduction problem, falls into the second category. At the current stage, we solved this problem for a large class of systems and the methods we developed lead to many interesting applications, which we will summarize in this proposal.

This thesis proposal is organized as follows: In the next section, we provide a general problem summary with an emphasis on the symmetry reduction. The problem summary is followed by a review of several branches of literature that are relevant to the proposed study in Sect. 1.2. Sect. 2.1 summarizes the first Fourier mode slice, which is the symmetry reduction method developed in the course of this study. We then present in Sect. 2.2 and Sect. 2.3 the applications of first Fourier mode slice to two problems with increasing difficulty. In Sect. 2.2, we extend the study of the dynamical system further to computation of all periodic orbits and cycle averages. Finally, in Sect. 3.1, we give a perspective for the future work regarding the application of afore mentioned methods to dynamics of incompressible fluid flow in a pipe.

1.1 Problem summary

In this thesis, we are going to study fields

$$\mathbf{u}(\mathbf{x},\tau)\,, \tag{1}$$

dynamics of which are determined by nonlinear PDEs. In the most general case, (1) is a three dimensional vector field, defined over the three dimensional configuration space $\mathbf{x}$ and time τ. Our approach is going to be bottom-up: Before attacking nonlinear PDEs, we are going to study the two-mode system, which mimics the symmetry structure of a scalar field in one space dimension under periodic boundary condition. Next, we are going to study Kuramoto-Sivashinsky system, which will be a one dimensional vector field defined over one space dimension and time. Finally, we are going to apply the methods we developed to the solutions of Navier-Stokes equations for incompressible fluid in a pipe.

Our goal in this thesis is to shine light into the dynamics of turbulence in simplest possible settings; in periodic computational domains only large enough to produce complicated dynamics. The geometrical simplicity of problems allows us to compute their solutions with high numerical accuracy by spectral methods. However, such simplicity comes at a cost: As

a consequence of periodicity, problems have continuous symmetries, hence their solutions have infinitely many copies. Consider, for simplicity, 1+1 dimensional field $u(x,\tau)$ under periodic boundary condition $u(x,\tau) = u(x+L,\tau)$. If the governing PDEs preserve their shape under a spatial shift $x \to x+\xi\,, \quad \xi \in (0,L)$, then each solution $u(x,\tau)$ has infinitely many copies that can be obtained by its translations $u(x+\xi,\tau)$. Expanding solutions in Fourier series

$$u(x,\tau) = \sum_{k=-\infty}^{\infty} \tilde{u}_k\,(\tau)\, e^{ikx}, \quad \tilde{u}_k = a_k + ib_k \tag{2}$$

and truncating at a large but finite N to meet a specified numerical accuracy, we can write a state space vector

$$a = (b_1, c_1, b_2, c_2, \ldots, b_N, c_N)\,, \tag{3}$$

for which the dynamics can be written as set of ordinary differential equations (ODEs)

$$\dot{a} = v(a)\,, \tag{4}$$

in state space $\mathcal{M}$ ($a \in \mathcal{M}$). In (3) we assumed that the field $u(x,\tau)$ is real valued and exhibits *Galilean invariance*, hence the $k > 0$ part of the spectrum is enough to completely describe its dynamics.

Fourier expansion (2) implies that translations in configuration space $u(x,\tau) \to u(x+\xi,\tau)$ are represented in the state space (3) as SO(2) rotations $a \to D(\theta)a$, with the matrix representation

$$D(\theta) = \mathrm{diag}\,[\,R(\theta),\, R(2\theta),\, \ldots,\, R(N\theta)\,]\,, \tag{5}$$

where

$$R(k\theta) = \begin{pmatrix} \cos k\theta & -\sin k\theta \\ \sin k\theta & \cos k\theta \end{pmatrix} \quad \text{and} \quad \theta = 2\pi\delta x/L\,. \tag{6}$$

The *symmetry reduction* problem is finding a coordinate transformation

$$\hat{a}(\tau) = \mathbf{S}[a(\tau)] \tag{7}$$

such that $\hat{a}$ is invariant under $a \to D(\theta)a$. This will allow us to have a unique representative for each symmetry related solution. Furthermore, in the reduced state space, high dimensional coherent solutions such as relative equilibria and relative periodic orbits will respectively become equilibria and periodic orbits. This will enable us to study the invariant manifolds of these coherent solutions and how those manifolds partition state space into qualitatively different regions. This will lead us to determine all periodic solutions of the system and to make quantitative predictions of the long term dynamics using periodic orbit theory. For the two-mode system, we have completed all these steps and described in Sect. 2.2. In Kuramoto-Sivashinsky system at the current stage, we are in the progress of investigating the unstable manifolds of invariant solutions. Application of these techniques to turbulent pipe flow is the future work of this thesis.

1.2 Literature review

In this section, we reviewed key developments and highlights in the literature related to this thesis. `ChaosBook.org` [12] offers a textbook introduction to most of these topics.

Modern dynamical theory of turbulence is a relatively new research field, largely driven by the computational advances of the last few decades. From a dynamical systems viewpoint, turbulence is a chaotic motion in the infinite dimensional state space, shaped by the

invariant solutions of the Navier-Stokes equations. This viewpoint was first articulated in 1948 by Hopf [25], however, it took more than 40 years for researchers to start to numerically find exact coherent solutions of Navier-Stokes equations [31]. Since then, many groups started to compute equilibria, traveling wave, periodic, and relative periodic solutions of plane Couette flow [32; 28; 43] and pipe flow [18; 44; 45]. In addition to computation of the exact coherent solutions, Gibson *et al.* [22] discovery and low dimensional visualizations of heteroclinic connections in the plane Couette flow is one of the most significant developments in the dynamical description of turbulence. Recently, Willis *et al.* [47] reported the discovery of more than 30 relative periodic orbits for the pipe flow, made possible by the first Fourier mode slice symmetry-reduction technique developed by Budanur *et al.* [8] (a key part of this thesis).

From the dynamical systems point of view, both plane Couette flow and pipe flow are chaotic systems with continuous and discrete symmetries, i.e. equivariant systems. According to Cushman, Bates [10] and Yoder [49], C. Huygens [26] understood the relative equilibria of a spherical pendulum many years before publishing them in 1673. Earliest modern study of such a problem known to us is Poincaré's work on the three-body problem [33]. More recent notable early works on the equivariant systems are those of Smale [42], Field [19], and Ruelle [36]. For a more detailed review of the literature, see ref. [12].

In the equivariant dynamics literature, a commonly used tool for local invariant description of dynamics is the method of slices, which will also be a central tool of this thesis. In the pure differential geometry context, method of slices (or method of 'moving frames') was introduced by Cartan [9], and early uses of slicing techniques in the dynamical systems that we know of are works of Field [20] and Krupa [29]. Our use of slicing techniques in this thesis closely follows the presentations of ref. [35], which applied the method to a traveling wave solution of the Kuramoto-Sivashinsky equation, and ref. [4], which applied the method to spiral waves. In ref. [21], Froehlich and Cvitanović study the singularity of the hyperplane slicing methods. Following their work Budanur *et al.* [8] realized that with a simple and natural choice of slice hyperplane for compact SO(2) symmetry, this singularity may be avoided for state space regions of interest. This work showed that it is possible to construct a global symmetry invariant description for systems with compact SO(2) symmetries and set the ground for the studies of their invariant manifolds.

The long-term goal of this research program, which this thesis is going to follow, is to make quantitative predictions about turbulent fields using periodic orbit theory. Foundational ideas behind the periodic orbit theory goe as far back as Poincaré's geometric approach to the three body problem [33], and Birkhoff's proof of the ergodic theorem [5]. The key developments we here are seminal works of Smale [41], Sinai [39], Bowen [6], and Ruelle [37]; where the mathematical foundations of thermodynamic approach to the deterministic chaotic dynamics can be found. Following a different path Gutzwiller arrived at the periodic orbit sum formulas for the energy spectrum of the quantum mechanical systems [23; 24]. Both classical and quantum mechanical trace formulas had problematic convergence, until Cvitanović [11] and Artuso *et al.* [2] realized that one obtains fast convergence if the cycles are ordered according to their topological lengths. They showed that topological ordering of cycles in dynamical zeta functions yields terms, where longer cycles are shadowed by the pseudocycles formed by shorter ones. Later on, Rugh proved that when one has hyperbolicity and finite grammar rules, cycle expansions of spectral determinant converges super-exponentially [38]. These theoretical advances were followed by many applications; among those, some notable examples are Artuso *et al.* applications to low-dimensional systems [3], cycle expansions for deterministic diffusion in the Lorentz gas [14],

Wintgen and collaborators semiclassical cycle expansions for the helium atom [17; 48]. To the best of our knowledge, first application of periodic orbit theory on a system with continuous symmetry were carried out by Budanur *et al.* [7], as a part of this thesis.

CHAPTER II

CURRENT STAGE

2.1 First Fourier mode slice

We stated in Sect. 1.1 that the first problem to be addressed in this thesis is the reduction of SO(2) symmetry; finding a transformation (7) such that resulting coordinates are symmetry invariant. We achieve this goal by a simple phase-fixing transformation, which we will first state in terms of complex Fourier modes: In the complex representation, the symmetry group is U(1)

$$\tilde{u}_k \to e^{ik\theta}\,\tilde{u}_k\,. \tag{8}$$

Now consider the time-dependent phase-fixing transformation

$$\hat{u}_k(\tau) = e^{-ik\arg\tilde{u}_1(\tau)}\tilde{u}_k(\tau)\,, \tag{9}$$

which fixes the phase of the first complex Fourier mode to 0 at all times. Hence, reduced Fourier modes $\hat{u}_k$ are invariant under (8). Notice however that we can make a transformation like (9) only if we have first Fourier mode $\tilde{u}_1$ non-vanishing. In what follows, we are going to show by using method of slices that $|\tilde{u}_1| = 0$ is a singularity of the symmetry reduced dynamics and we can regularize this for arbitrarily small $|\tilde{u}_1|$ by a time-rescaling.

In order to introduce method of slices, let us first repose the symmetry reduction problem in a geometrical setting. We define the *group orbit* of a state a as the set of states, which can be reached from a by group transformations

$$\mathcal{M}_{D(\theta)a} = \{D(\theta)\,a \mid \theta \in [0, 2\pi)\}\,. \tag{10}$$

We now define the *slice* as a submanifold $\hat{\mathcal{M}} \subset \mathcal{M}$, which is cut by every group orbit in an open neighborhood of (10) only once. Each such intersection is then thought as the *representative* of the respective group orbit, hence the symmetry is reduced within the slice.

The abstract definition of a slice is not very useful, until we have a way of constructing it. In practice, one defines a *slice hyperplane* as the hyperplane of points $\hat{a}$ defined by

$$\langle \hat{a} - \hat{a}'|t'\rangle = 0 \quad \text{and} \quad \langle t(\hat{a})|t'\rangle > 0\,, \tag{11}$$

where $t(\hat{a}) = T\hat{a}$ is the group tangent at $\hat{a}$, $t' = t(\hat{a}')$ is the slice tangent and T is the Lie algebra generator satisfying $D(\theta) = e^{\theta T}$. In (11), the state space point $\hat{a}'$ is called the slice template, which defines the slice hyperplane as the set of points which are orthogonal to its group tangent t', i.e. *template tangent*. For orthogonal groups, by definition $\langle \hat{a}'|t'\rangle = 0$, hence the first condition in (11) reduces to $\langle \hat{a}|t'\rangle = 0$. The second condition in (11) is a directional constraint that picks one of the two intersections of the group orbit with the slice hyperplane. With these definitions, the symmetry reduction problem becomes finding time dependent group parameter $\theta(\tau)$, which brings the trajectory $a(\tau)$ to the slice hyperplane as illustrated in Figure 1. Dynamics within the slice hyperplane and in the full state space are then related by

$$\hat{a}(\tau) = D(-\theta(\tau))\,a(\tau)\,, \tag{12}$$

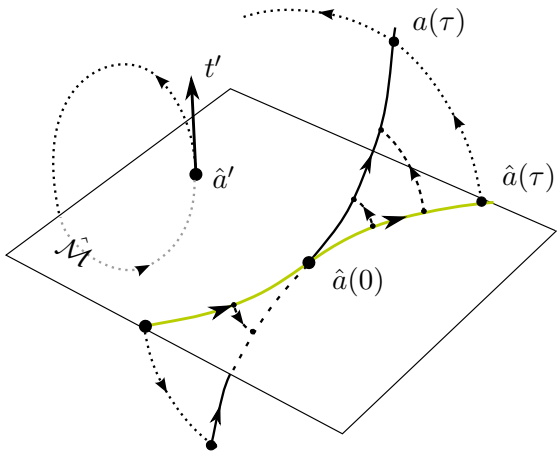

Figure 1: The slice hyperplane $\hat{\mathcal{M}}$, which passes through the template point $\hat{a}'$ and is normal to its group tangent t', intersects all group orbits (dotted lines) in an open neighborhood of $\hat{a}'$. The full state space trajectory $a(\tau)$ (solid black line) and the reduced state space trajectory $\hat{a}(\tau)$ (solid green line) belong to the same group orbit $\mathcal{M}_{a(\tau)}$ and are equivalent up to a 'moving frame' rotation by phase $\theta(\tau)$. Adapted from ChaosBook.org.

and the group parameter $\theta(\tau)$ defines the *moving frame*.

It is also possible to investigate dynamics directly within the slice hyperplane determined by ODEs

$$\dot{\hat{a}} = \hat{v}(\hat{a})\,, \tag{13}$$

where $\hat{v}(\hat{a})$ is given by

$$\hat{v}(\hat{a}) = v(\hat{a}) - \dot{\theta}(\hat{a})\, t(\hat{a})\,, \tag{14}$$

$$\dot{\theta}(\hat{a}) = \langle v(\hat{a})|t'\rangle / \langle t(\hat{a})|t'\rangle\,. \tag{15}$$

The reconstruction phase $\theta(\tau)$ can also be computed by integrating (15), and thus one can go back and forth between full state space and the slice by (12). We can see from (15) that the phase velocity becomes singular if $\langle t(\hat{a})|t'\rangle$ vanishes. This makes the slice hyperplane a local symmetry reduction method, and its border $\hat{a}^*$ is defined by

$$\langle t(\hat{a}^*)|t'\rangle = 0\,. \tag{16}$$

We are now going to focus back on the SO(2) case and show that this problem can be avoided in many practical cases for a special choice of the slice template. The infinitesimal generator of the group action (5) is

$$T = \mathrm{diag}\,[\,T_1,\, T_2,\, \ldots,\, T_N\,]\,, \quad \text{where} \quad T_k = \begin{pmatrix} 0 & -k \\ k & 0 \end{pmatrix}\,. \tag{17}$$

Now if we choose a slice template as

$$\hat{a}' = (1, 0, 0, \ldots, 0)^T\,, \tag{18}$$

the corresponding template tangent is

$$t' = (0, 1, 0, \ldots, 0)^T\,, \tag{19}$$

hence (11) for this specific choice becomes

$$c_1 = 0 \quad \text{and} \quad b_1 > 0\,, \tag{20}$$

which is the real-valued representation equivalent of the phase-fixing transformation (9). If we now rewrite the phase velocity (15) explicitly for this choice as

$$\dot\theta(\hat a) = \dot c_1/\hat b_1\,, \tag{21}$$

we see that it is singular when $\hat b_1 = 0$. We regularize this by defining the *slice time* as

$$d\hat\tau = d\tau/\hat b_1\,, \tag{22}$$

which regularizes this singularity as the reduced dynamics with respect to the slice time is defined by

$$\begin{aligned} d\hat a/d\hat\tau &= \hat b_1 v(\hat a) - \dot c_1(\hat a)\, t(\hat a)\,, &(23)\\ d\theta(\hat a)/d\hat\tau &= \dot b_1(\hat a)\,. &(24)\end{aligned}$$

We call this method *first Fourier mode slice*, since the effect of this transformation is fixing the phase of the first Fourier mode to 0 as in (9). In the following sections, we will discuss some applications.

2.2 Two-mode system

In Sect. 1.1, we explained that the study of nonlinear PDEs under periodic boundary conditions is the study of infinite dimensional dynamical systems with continuous symmetries. In particular, we showed that translation symmetry in one space direction implies SO(2) rotations in the corresponding Fourier representation and in the previous section, we presented a method for reducing this symmetry. As a first application, we pick the dimensionally simplest setting, namely the two-mode SO(2)-equivariant ODE normal form

$$\begin{aligned} \dot z_1 &= (\mu_1 - i\,e_1)\, z_1 + a_1\, z_1|z_1|^2 + b_1\, z_1|z_2|^2 + c_1\, \overline{z}_1\, z_2\,,\\ \dot z_2 &= (\mu_2 - i\,e_2)\, z_2 + a_2\, z_2|z_1|^2 + b_2\, z_2|z_2|^2 + c_2\, z_1^2\,. \end{aligned} \tag{25}$$

In (25), (z_1, z_2) are complex state space coordinates, $\overline{z}_i$ denotes complex conjugation, and $a_{1,2}, b_{1,2}, c_{1,2}, e_{1,2}, \mu_{1,2}$ are system parameters. Two-mode system ODEs (25) preserve their form under U(1) transformation

$$(z_1, z_2) \to (e^{i\phi} z_1, e^{i2\phi} z_2)\,, \tag{26}$$

Thus, in the real valued state space $a = (x_1, y_1, x_2, y_2)$, where $z_j = x_j + iy_j$, we have SO(2) symmetry

$$v(D(\theta)\, a) = D(\theta)\, v(a)\,, \tag{27}$$

where $D(\theta)$ defined as in (5) with $N = 2$.

Parameters $e_{1,2}$ have a special meaning. If they are equal to 0, then we get an additional symmetry under complex conjugation $(z_1, z_2) \to (\overline{z}_1, \overline{z}_2)$, and the symmetry in the real representation becomes O(2). Dangelmayr [15], Armbruster, Guckenheimer and Holmes [1], and Jones and Proctor [27] studied bifurcations of (25) in the O(2)-equivariant setting;

and Porter and Knobloch [34] studied the non-zero e_i case. We study (25) far from its bifurcations, and in what follows the parameters are set to

μ_1	μ_2	e_1	e_2	a_1	a_2	b_1	b_2	c_1	c_2
-2.8	1	0	1	-1	-2.66	0	0	-7.75	1

(28)

For clarity of the presentation, we rewrite the two-mode ODEs in the real representation, omitting the parameters that are set to 1 or 0 in (28)

$$\begin{aligned}
\dot{x}_1 &= (\mu_1 - r_1^2 + x_2)x_1 + y_1 y_2 \,, \\
\dot{y}_1 &= (\mu_1 - r_1^2 - c_1 x_2)y_1 + c_1 x_1 y_2 \,, \\
\dot{x}_2 &= (1 + a_2 r_1^2)x_2 + (x_1^2 - y_1^2) + y_2 \,, \\
\dot{y}_2 &= (1 + a_2 r_1^2)y_2 + 2x_1 y_1 - x_2 \,, \\
&\text{where } r_1^2 = x_1^2 + y_1^2 \,, \quad r_2^2 = x_2^2 + y_2^2 \,, \\
&\mu_1 = -2.8 \,,\, a_2 = -2.66 \,,\, c_1 = -7.75 \,.
\end{aligned} \tag{29}$$

As a first demonstration of utility of the symmetry reduction Figure 2 shows three trajectories of the two-mode system (29) in original and symmetry reduced representations. Notice that the slice condition (11) along with the choice of the first Fourier mode slice template (18) sets $\hat{y}_1 = 0$, thus the reduced state space visualization Figure 2 (b) shows entire dynamical information whereas Figure 2 (a) is a $3D$ projection of the original $4D$ state space.

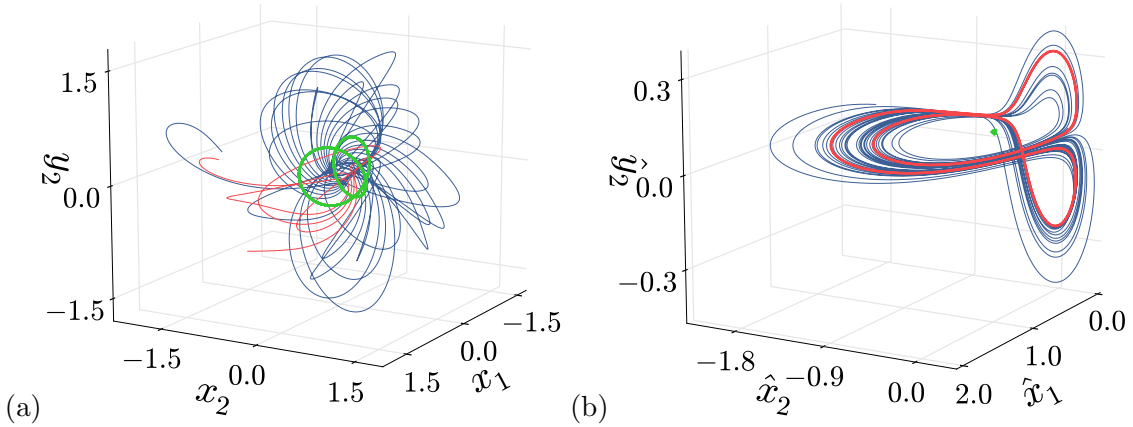

Figure 2: The relative equilibrium (green), relative periodic orbit $\overline{01}$ (red), and an ergodic trajectory (blue) of the two-mode system (29) in (a) in a 3D projection of the 4-dimensional state space, (b) in the 3-dimensional first Fourier mode slice hyperplane. Note that in the symmetry reduced representation (b), the relative equilibrium TW is reduced to an equilibrium, the green point; and the periodic orbit $\overline{01}$ (red) closes onto itself after one repeat. Adapted from [7].

As Figure 2 clearly demonstrates that once the continuous symmetry is reduced, resulting dynamics is governed by a thin chaotic attractor. This attractor is in fact shaped by the invariant manifolds of two equilibria of the symmetry reduced dynamics. First of these two equilibria is located at the origin and it is an equilibrium of the original system (29). In fact, the origin $a = 0$ do not satisfy the slice condition (11), yet it still plays the role of shaping the invariant dynamics as its stable and unstable manifolds enter the slice. Linear

stability at the origin is determined by the stability matrix $A_{ij}(0) = \partial v_i/\partial a_j|_{a=0}$ formed by the partial derivatives of the RHS of the (29). $A(0)$ is diagonal with eigenvalues $\lambda_{1,2} = -2.8$ corresponding to x_1, y_1 directions, and $\lambda_{3,4} = 1$ corresponding to x_2, y_2 directions. Second equilibrium of the reduced dynamics is a relative equilibrium, shown green in Figure 2. We locate this relative equilibrium by solving for the roots of (14) as

$$(x_1, y_1, x_2, y_2)_{\mathrm{TW}} = (0.439966, 0, -0.386267, 0.070204)\ . \tag{30}$$

Similarly, we determine the linear stability of this equilibrium by reduced stability matrix $\hat{A}_{ij}(\hat{a}_{\mathrm{TW}}) = \partial \hat{v}_i/\partial \hat{a}_j|_{\hat{a}_{\mathrm{TW}}}$, whose eigenvalues are

$$\lambda_{1,2} = 0.05073 \pm i\, 2.4527, \quad \lambda_3 = -5.5055, \quad \lambda_4 = 0\,. \tag{31}$$

0 eigenvalue of the reduced stability matrix corresponds to the direction pointing outside the slice. The complex pair $\lambda_{1,2}$ indicates a 2-dimensional unstable manifold of the relative equilibrium with spiraling-out dynamics, and the large negative eigenvalue λ_3 corresponds to the direction pointing outside the attractor.

We reduce the two-mode dynamics further down to a unimodal return map by investigating the Poincaré section hyperplane, which we construct by following the unstable manifold of the relative equilibrium $\hat{a}_{\mathrm{TW}}$ as shown in Figure 3. We collect the data for the return map in Figure 3 (b) by measuring the arclengths along the Poincaré section curve interpolating the intersections in Figure 3 (a). Cubic spline interpolation to this data results in the Poincaré return map of Figure 3 (b).

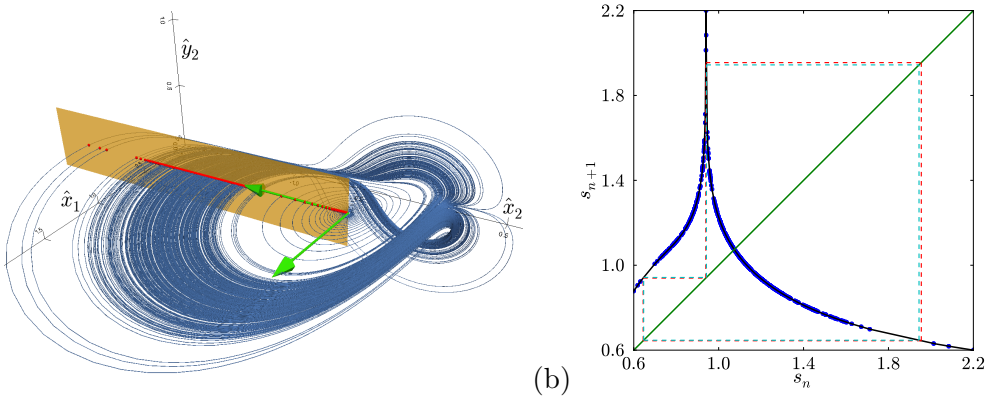

(a) (b)

Figure 3: (a) A Symmetry-reduced ergodic trajectory within the slice hyperplane (blue). Green arrows indicate the real and imaginary parts of the complex eigenvectors v_u that span the unstable manifold of TW. The Poincaré section, which contains TW and is spanned by $\mathrm{Im}\,[v_u]$ and $\hat{y}_2$, is visualized as a transparent plane. Points where the flow crosses the section are marked in red. (b) By measuring arclengths s along the interpolation curve, a return map of the Poincaré section can be constructed. The flow exits the neighborhood of the TW ($s < 0.6$) it stays on the attractor and never comes back. Thus the data up to this point is transient, and omitted in (b). Dashed lines show the 3-cycles $\overline{001}$ (red) and $\overline{011}$ (cyan). Adapted from [7].

Having a unimodal return map enables us to determine all admissible relative periodic orbits of the two-mode system, along with their symbolic dynamics. Notice, however, that the return map in Figure 3 (b) has a sharp cusp, at the tip of which we have the furthest intersection of the trajectory in Figure 3 (a) with the Poincaré section. In principle, this

cusp may extend further, and more and more cycles can be accessible in the Poincaré map as this cusp gets sharper. However, all those cycles are increasingly unstable, hence they are both hard to find numerically and they are less important for periodic orbit theory calculations. For this reason, we assume that the tip of the cusp in Figure 3 as the critical point of the return map, and do not search for the relative periodic orbits whose topological coordinates are above the *kneading value* computed for this point. For an n-cycle, the we find n arc-lengths $\{s_0, s_1, \ldots s_n\}$ from the return map, and we convert these arc-lengths to corresponding reduced state space coordinates $\{\hat{a}_0, \hat{a}_1, \ldots \hat{a}_n\}$. We then integrate (14) and (15) for each of these points for one Poincaré return to obtain guesses for the period and the phase shift of the relative periodic orbit; and finally, feed these into a multiple shooting Newton solver to bring the numerical accuracy of the relative periodic orbit to our working precision 10^{-9}. In order to compute the Floquet spectrum of each relative periodic orbit accurately, we employ Periodic Schur decomposition as described in ref. [16]. Figure 4 shows the four shortest relative periodic orbits found for the two-mode system (29) (a) and distribution of positive Floquet exponents for all relative periodic orbits found up to topological length 12 (b). We have also listed the symbolic itineraries, periods, phase shifts, and largest Floquet multipliers and exponents for relative periodic orbits with topological lengths up to $n = 5$, in Table 1. As can be seen from Figure 3 (b) and Figure 4 (a) that cycles $\overline{001}$ and $\overline{011}$ overlap almost everywhere in the state space but they have topologically distinct properties. As one can see from Figure 4 (b), their Floquet exponents are also almost equal, however, their leading Floquet multipliers have different signs reflecting their topological distinction, see Table 1.

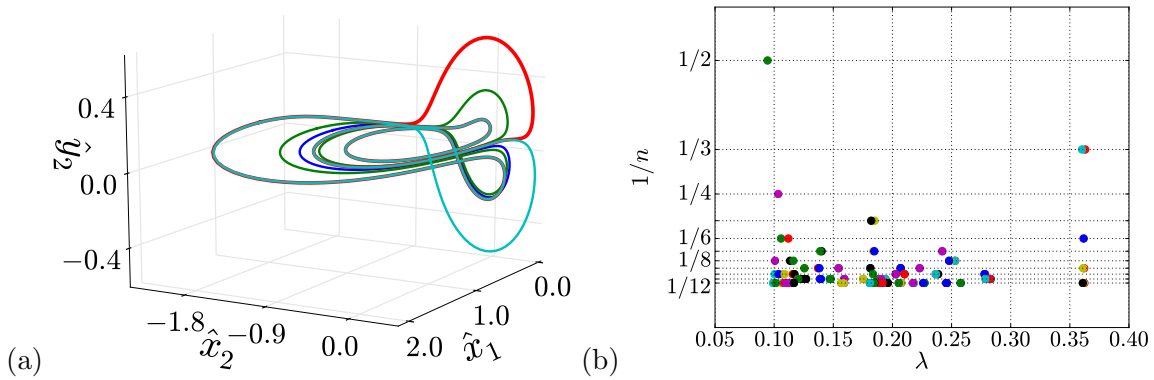

Figure 4: (a) Shortest four relative periodic orbits of the two-mode system: $\overline{1}$ (dark blue), $\overline{01}$ (green), $\overline{001}$ (red), $\overline{011}$ (cyan). Note that relative periodic orbits $\overline{001}$ and $\overline{011}$ almost overlap everywhere except $\hat{x}_1 \approx 0$. (b) Distribution of the expanding Floquet exponents of all two-mode cycles with topological lengths n from 2 to 12. Adapted from [7].

We conclude our study of the two-mode system by carrying out periodic orbit theory calculations using the relative periodic orbits we found. For this purpose, we construct the spectral determinant

$$\det(s - \mathcal{A}) = \prod_p \exp\left(- \sum_{r=1}^{n_p r < N} \frac{1}{r} \frac{e^{r(\beta \Omega_p - s T_p)}}{\left|\det\left(\mathbf{1} - M_p^r\right)\right|} z^{n_p r} \right) , \tag{32}$$

where $\mathcal{A}$ is the generator of the Perron-Frobenius type evolution operator associated with an observable ω, p denotes prime periodic orbits and r sum is over their repeats, β is an

Table 1: Itinerary, period (T), phase shift (θ), Floquet multiplier (Λ), and Floquet exponent (λ) of the found two-mode relative periodic orbits with topological lengths up to $n = 5$. Adapted from [7].

Itinerary	T	θ	Λ	λ
1	3.64151221	0.08096967	-1.48372354	0.10834917
01	7.34594158	-2.94647181	-2.00054831	0.09439516
001	11.07967801	-5.64504385	-55.77844510	0.36295166
011	11.07958924	-2.50675871	54.16250810	0.36030117
0111	14.67951823	-2.74691247	-4.55966852	0.10335829
01011	18.39155417	-5.61529803	-30.00633820	0.18494406
01111	18.38741006	-2.48213868	28.41893870	0.18202976

auxiliary variable, Ω_p is the integrated value of the observable ω over the prime periodic orbit$p$, T_p is the period of the periodic orbit p, and M_p is the transverse monodromy matrix, eigenvalues of which are the non-marginal Floquet multipliers associated with the prime periodic orbit p. The order tracking parameter z is set to 1 after (32) is expanded to a certain order N in z. We will denote the Nth order approximation to the spectral determinant computed this way by $F_N(\beta, s)$.

Long time average $\langle\omega\rangle$ of an observable ω and its associated diffusion coefficient Δ is related to the eigenvalues $s(\beta)$ as follows

$$\begin{aligned} \langle\omega\rangle &= \lim_{\tau\to\infty}\frac{1}{\tau}\langle\Omega^\tau\rangle = \left.\frac{\partial s(\beta)}{\partial\beta}\right|_{\beta=0}, \\ \Delta &= \lim_{\tau\to\infty}\frac{1}{\tau}\langle(\Omega^\tau)^2 - \langle\Omega^\tau\rangle^2\rangle = \left.\frac{\partial^2 s(\beta)}{\partial\beta^2}\right|_{\beta=0}. \end{aligned} \tag{33}$$

We obtain these eigenvalues from the N-th order spectral determinant $F_N(\beta, s)$ by taking derivatives of the implicit equation

$$F(\beta, s(\beta)) = 0\,. \tag{34}$$

Defining

$$\begin{aligned} \langle\Omega\rangle &= -\partial F/\partial\beta \\ \langle T\rangle &= \partial F/\partial s\,, \qquad \langle T^2\rangle = \partial^2 F/\partial s^2 \\ \langle\Omega^2\rangle &= -\partial^2 F/\partial\beta^2\,, \qquad \langle\Omega T\rangle = \partial^2 F/\partial\beta\partial s\,, \end{aligned} \tag{35}$$

We write the cycle averaging formulas as

$$\langle\omega\rangle = \langle\Omega\rangle/\langle T\rangle\,, \tag{36}$$

$$\begin{aligned} \Delta &= \frac{1}{\langle T\rangle}\left(\langle\Omega^2\rangle - 2\frac{ds}{d\beta}\langle\Omega T\rangle + \left(\frac{ds}{d\beta}\right)^2\langle T^2\rangle\right) \\ &= \frac{1}{\langle T\rangle}\langle(\Omega - T\langle\omega\rangle)^2\rangle\,. \end{aligned} \tag{37}$$

with everything evaluated at $\beta = 0$, $s = s(0)$.

We evaluated the cycle averaging formulas for the Lyapunov exponent and the average phase velocity by setting $\Omega_p = \ln|\Lambda_{p,e}|$, and $\Omega_p = \theta_p$ respectively. In addition, we have also computed the phase diffusion constant, which we defined as

$$D = \frac{1}{2d}\lim_{\tau\to\infty}\frac{1}{\tau}\langle\theta(\tau)^2 - \langle\theta(\tau)\rangle^2\rangle\,, \tag{38}$$

where $d = 1$ since phase velocity is analogous to the drifts in a one dimensional configuration space.

We mentioned in the literature review of Sect. 1.2 that cycle expansions of the spectral determinants converge super-exponentially when the symbolic dynamics has finite number of grammar rules [38]. With this in mind, we decided to introduce a cut-off to the cusp of the return map in Figure 3 such that the remaining cycles obey *golden mean grammar*, namely we drop all cycles with symbol sequence 00, assuming the cusp of the return map ends at the point it is cut by $\overline{001}$. We named this "finite grammar approximation" and carried out our calculations within and without it for comparison. Cycle averages with respect to expansion order within and without the finite grammar approximation are listed in Table 2 and Table 3 respectively. Notice that the finite grammar approximation improves the convergence of cycle expansions significantly for every observable. In particular, we have six converging digits in the diffusion constant D in Table 2, whereas without the golden mean grammar number of converging digits is three.

Table 2: Cycle expansion estimates for the escape rate γ, average cycle period $\langle T\rangle$, Lyapunov exponent λ, average phase velocity $\langle\dot{\theta}\rangle$, and the diffusion coefficient D, using cycles up to length N in the finite grammar approximation. Adapted from [7].

N	γ	$\langle T\rangle$	λ	$\langle\dot{\phi}\rangle$	D
1	0.249829963	3.6415122	0.10834917	0.0222352	0.000000
2	-0.011597609	5.8967605	0.10302891	-0.1391709	0.143470
3	0.027446312	4.7271381	0.11849761	-0.1414933	0.168658
4	-0.004455525	6.2386572	0.10631066	-0.2141194	0.152201
5	0.000681027	5.8967424	0.11842700	-0.2120545	0.164757
6	0.000684898	5.8968762	0.11820050	-0.1986756	0.157124
7	0.000630426	5.9031596	0.11835159	-0.1997353	0.157345
8	0.000714870	5.8918832	0.11827581	-0.1982025	0.156001
9	0.000728657	5.8897511	0.11826873	-0.1982254	0.156091
10	0.000728070	5.8898549	0.11826788	-0.1982568	0.156217
11	0.000727891	5.8898903	0.11826778	-0.1982561	0.156218
12	0.000727889	5.8898908	0.11826780	-0.1982563	0.156220

With these results, we conclude our study of the two-mode system. While it is merely a toy-problem, the two-mode system thought us several important lessons: First of all, the symmetry reduction is absolutely crucial to understand the attractor geometry of the systems with continuous symmetries. Moreover, we can use relative periodic orbits to accurately compute observable averages for these systems. Finally, the topological properties of the system are very important for the convergence of cycle averaging calculations.

Table 3: Cycle expansion estimates of the escape rate γ, average cycle period $\langle T \rangle$, Lyapunov exponent λ, average phase velocity $\langle \dot{\theta} \rangle$, and the diffusion coefficient D with respect expansion order using cycles up to length N. Adapted from [7].

N	γ	$\langle T \rangle$	λ	$\langle \dot{\phi} \rangle$	D
1	0.249829963	3.6415122	0.10834917	0.0222352	0.000000
2	-0.011597609	5.8967605	0.10302891	-0.1391709	0.143470
3	0.022614694	4.8899587	0.13055574	-0.1594782	0.190922
4	-0.006065601	6.2482261	0.11086469	-0.2191881	0.157668
5	0.000912644	5.7771642	0.11812034	-0.2128347	0.168337
6	0.000262099	5.8364534	0.11948918	-0.2007615	0.160662
7	0.000017707	5.8638210	0.12058951	-0.2021046	0.160364
8	0.000113284	5.8511045	0.12028459	-0.2006143	0.159233
9	0.000064082	5.8587350	0.12045664	-0.2006756	0.158234
10	0.000093124	5.8536181	0.12035185	-0.2007018	0.158811
11	0.000153085	5.8417694	0.12014700	-0.2004520	0.158255
12	0.000135887	5.8455331	0.12019940	-0.2005299	0.158465

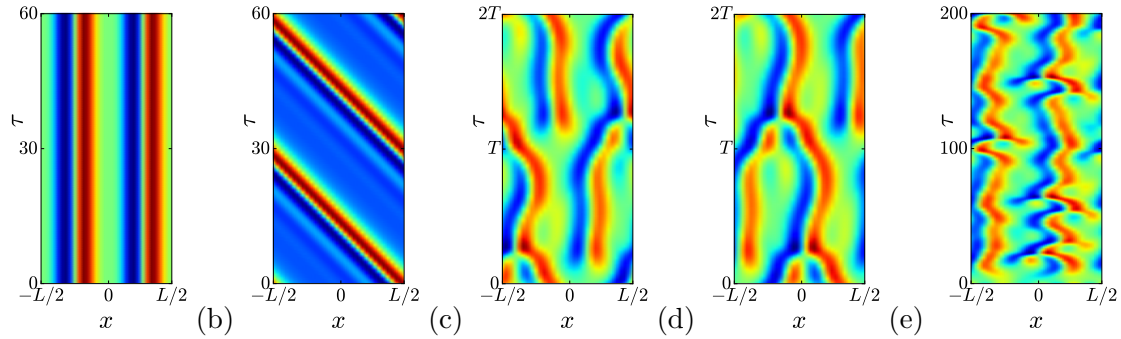

Figure 5: Examples of coherent solutions of the Kuramoto-Sivashinsky system and the ergodic flow visualized as the color coded amplitude of the scalar field $u(x, \tau)$: (a) Equilibrium E_1 (b) Relative equilibrium TW_1 (c) Pre-periodic orbit with period $T = 32.4$. (d) Relative periodic orbit with period $T = 33.5$ (e) Ergodic flow. Horizontal and vertical axes correspond to space and time respectively.

2.3 Kuramoto-Sivashinsky system

The second problem we study is the Kuramoto-Sivashinsky equation in one space dimension

$$u_\tau = -\tfrac{1}{2}(u^2)_x - u_{xx} - u_{xxxx}\,, \tag{39}$$

with periodic boundary condition $u(x, \tau) = u(x + L, \tau)$. The scalar field $u(x, t)$ describes the velocity of a turbulent flame front [40]. The length L is the Reynolds' parameter for system, which exhibits spatiotemporal chaos for sufficiently large system sizes. We set the system size to $L = 22$ as done in ref. [13], where the coherent solutions we are going to use were found. Figure 5 shows configuration space visualizations of four of these solutions along with a typical spatiotemporally chaotic trajectory.

We start constructing the state space of the Kuramoto-Sivashinsky system by Fourier expanding solutions as in (2) and expressing (39) in terms of Fourier modes as an infinite

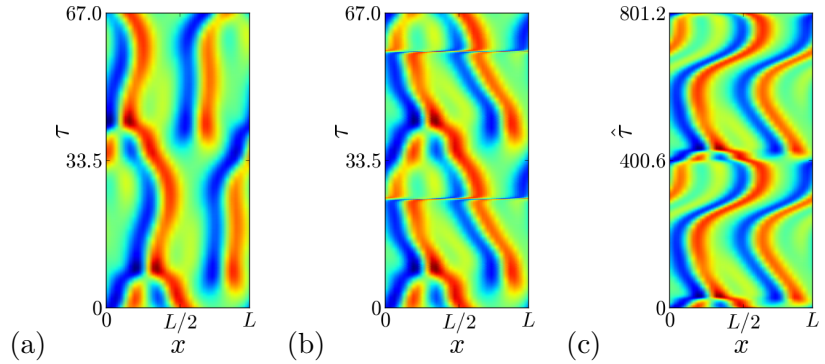

Figure 6: Relative periodic orbit $T_p = 33.50$ in configuration space: (d) the full state space solution, (e) symmetry-reduced solution with respect to the lab time, and (f) symmetry-reduced solution with respect to the in-slice time. Adapted from [8].

set of ODEs

$$\dot{\tilde{u}}_k = (q_k^2 - q_k^4)\,\tilde{u}_k - i\frac{q_k}{2}\sum_{m=-\infty}^{+\infty}\tilde{u}_m\tilde{u}_{k-m}\,, \quad q_k = \frac{2\pi k}{L}\,. \tag{40}$$

The Galilean invariance of the Kuramoto-Sivashinsky equation follows from (40) by observing that the zeroth Fourier mode $\tilde{u}_0$ is time-invariant. Hence, we exclude $\tilde{u}_0$ from the state space and construct the real valued state space vector for Kuramoto-Sivashinsky system as (3). Spatial translation is represented in the state space (3) by (5). In addition to translation, Kuramoto-Sivashinsky equation is also equivariant under the reflection $u(x,\tau) \to -u(-x,\tau)$, which has the matrix representation

$$D(R) = \mathrm{diag}\,[\,-1,\ 1,\ -1,\ 1,\ \ldots,\ -1,\ 1]\ . \tag{41}$$

in the state space (3). Coexistence of translation and reflection symmetries allows Kuramoto-Sivashinsky equation to have four types of exactly coherent solutions: Equilibria $a = f^\tau(a)$ (Figure 5 (a)), relative equilibria $D(\theta = c\tau)a = f^\tau(a)\,,\ c = \text{const.}$ (Figure 5 (b)), pre-periodic orbits $D(R)a = f^T(a)\,,\ T = \text{const.}$ (Figure 5 (c)), and relative periodic orbits $D(\theta)a = f^T(a)\,,\ T = \text{const.}\,,\theta = \text{const.}$ (Figure 5 (d)), where $f^\tau(a)$ denotes the finite-time flow mapping induced by dynamics. We began constructing a symmetry invariant description of the Kuramoto-Sivashinsky system by applying the first Fourier mode slice to reduce its continuous symmetry and we found that the regularized formulation (23) is an absolute necessity to ensure the smoothness of the reduced flow. This is illustrated in Figure 6, where we have shown two repeats of the Kuramoto-Sivashinsky relative periodic orbit with period $T_p = 33.50$ (a), along with its symmetry reduced visualizations with respect to lab time (b) and slice time (c). Figure 6 (c) clearly shows that what appears to be discrete jumps in the dynamics in Figure 6 (b) are in fact fast episodes of the dynamics close to the singularity of (15).

We have further reduced the remaining discrete symmetry of the Kuramoto-Sivashinsky system by means of invariant polynomials, which then allowed us to produce global visualization of the Kuramoto-Sivashinsky dynamics in the state space. These preliminary results are not included in this proposal due to length limitation.

CHAPTER III

PLANNED WORK

3.1 Navier-Stokes equations and the pipe flow

The last system we are going to study in this thesis, namely the turbulent dynamics of an incompressible fluid confined in a volume, is vastly more complicated than the previous two. Therefore, the results that are going to be presented in the last part of thesis will be outcomes of a collaborative effort of the groups in Georgia Tech, University of Sheffield, and University of New Hampshire. In what follows, we are going to remark on how some of the ideas summarized in the earlier parts of this proposal can be applied to fluid flows. Navier-Stokes equations for an incompressible fluid reads

$$\frac{\partial \mathbf{u}}{\partial \tau} + \mathbf{u}\cdot\nabla\mathbf{u} = -\frac{\nabla p}{\rho} + \nu\nabla^2\mathbf{u} + \mathbf{f}\,, \tag{42}$$

$$\nabla\cdot\mathbf{u} = 0\,, \tag{43}$$

where $\mathbf{u} = \mathbf{u}(\mathbf{x},\tau)$ denotes the velocity field of the fluid, $p = p(\mathbf{x},\tau)$ denotes pressure, $\mathbf{f}$ is the external forcing, such as gravity, in presence, and ρ and ν are the constant density and the viscosity of the fluid under study. We would like to study the dynamics of the velocity field determined by (42) and (43), for given initial condition and boundary conditions. The first complication we face is the question of how dynamics of the pressure field $p(\mathbf{x},t)$ is determined. Taking the divergence of (42) and using (43), we obtain

$$\nabla^2 p = \rho\,\nabla\cdot(\mathbf{f} - \mathbf{u}\cdot\nabla\mathbf{u})\,, \tag{44}$$

which, in principle, can be solved simultaneously with (42) with the boundary condition

$$\frac{\partial p}{\partial n} = \rho\,(\nu\nabla^2\mathbf{u} + \mathbf{f})\cdot\mathbf{n}\,, \tag{45}$$

where $\mathbf{n}$ is the normal vector on boundaries. A rather elegant method that eliminates both the pressure term and the incompressibility condition (43) from computations is the two-potential formulation of the problem, where one expresses the velocity field as

$$\mathbf{u} = \nabla\times(\psi\,\mathbf{e}) + \nabla\times\nabla\times(\phi\,\mathbf{e})\,, \tag{46}$$

where ψ and ϕ are scalar potentials and e is a constant vector chosen according to problem geometry. Plugging (46) into (42) yields equations for potentials ψ and ϕ, which can be solved with additional boundary conditions to determine the velocity field. Marques [30] showed the validity of this representation and derived formulas for the boundary conditions that the potentials must satisfy. This approach is adapted to pipe flow by Willis in openpipeflow.org and is described in ref. [46]. `openpipeflow` software is used for the computations that are going to be presented in this thesis.

Let us now consider specifically the flow of a fluid in a pipe with periodic boundary condition in the axial direction z and "no slip" boundary condition on the pipe wall

$$\begin{aligned}\mathbf{u}(r,\phi,z+L,\tau) &= \mathbf{u}(r,\phi,z,\tau)\,,\\ \mathbf{u}(r=R,\phi,z,\tau) &= 0\,.\end{aligned} \tag{47}$$

where L and R are the length and radius of the pipe. We can express each component of the velocity field as an expansion of the following form

$$u^{(i)}(r,\phi,z,\tau) = \sum_{n=1}^{\infty}\sum_{k=-\infty}^{\infty}\sum_{m=-\infty}^{\infty} u^{(i)}_{nkm} J_0(\alpha_n r)\, e^{i(kz+m\phi)}\,, \tag{48}$$

where i indexes three components of the velocity field, and α_n is determined from the nth root of the Bessel function, thus the expansion satisfies the boundary condition on the walls [1]. Considering a finite-mode truncation of the expansion (48), we can think of the pipe flow as a dynamical system in a state space where each dimension corresponds to one of the discretization elements $u^{(i)}_{nkm}$ in (48). In order to have a feeling of the dimensionality of this system, let us make a very rough estimate by assuming that for each dimension, we only take 16 modes as we did in the one dimensional Kuramoto-Sivashinsky problem, which would yield a $3\times16\times16\times16 = 12288$ complex modes. In reality, this number easily reaches the order of 10^5, and this fact by itself makes the study of turbulence very difficult.

As described in detail in ref. [45] symmetry group of the pipe flow is $\mathrm{O}(2)_\phi \times \mathrm{SO}(2)_z$, which includes the rotations and reflection in azimuthal direction, and shifts in axial direction. Reflection symmetry in z direction is broken by the net pressure gradient that is needed for retaining a net flux through the pipe. Reduction of these continuous symmetries can be performed by first Fourier mode slice method of Sect. 2.1 by picking two slice templates in the state space formed by the discretization (48) as

$$u'^{(1)}_{z,nkm} = \frac{\delta_{i,1}}{2}\left(\delta_{n,1}\delta_{k,1}\delta_{m,0} + \delta_{n,1}\delta_{k,-1}\delta_{m,0}\right)\,, \tag{49}$$

$$u'^{(1)}_{\phi,nkm} = \frac{\delta_{i,1}}{2}\left(\delta_{n,1}\delta_{k,0}\delta_{m,1} + \delta_{n,1}\delta_{k,0}\delta_{m,-1}\right)\,, \tag{50}$$

which respectively corresponds to picking states that have non-zero components only in the real part of the first mode in z and ϕ expansions. We have also arbitrarily chosen the first component of the velocity field for slice templates of (49) and (50), and we will investigate the effects of this choice in our applications. In a slightly different form, Willis *et al.* already implemented the first Fourier mode slice for the axial shift symmetry of the pipe flow [47] in the shift and reflect invariant subspace, where the azimuthal rotation symmetry is broken.

Continuous symmetry reduction enables Gibson *et al.*'s low dimensional visualization techniques for the unstable manifolds of traveling wave solutions, since they become equilibria in the reduced state space. By applying this, we are expecting to learn how these invariant manifolds organize turbulent solutions of the pipe flow. Moreover, since the reduction of continuous symmetries considerably simplifies the geometry of the state space, we are expecting to find more relative periodic orbits of the pipe flow, which may eventually lead to the quantitative predictions for physical observables such as laminarization times or energy dissipation rates. Another remaining task for the symmetry reduction of the pipe flow is the reduction of the azimuthal reflection symmetry. We have solved this problem for Kuramoto-Sivashinsky system by introducing invariant polynomials and we are currently developing a similar method for the pipe flow.

[1] `openpipeflow` uses finite difference methods for radial discretization of the problem for computational convenience. However, solutions can be brought to the form of (48) by post-processing the data.

Bibliography

[1] Armbruster, D., Guckenheimer, J., and Holmes, P., "Heteroclinic cycles and modulated travelling waves in systems with O(2) symmetry," *Physica D*, vol. 29, pp. 257–282, 1988.

[2] Artuso, R., Aurell, E., and Cvitanović, P., "Recycling of strange sets: I. Cycle expansions," *Nonlinearity*, vol. 3, pp. 325–359, 1990.

[3] Artuso, R., Aurell, E., and Cvitanović, P., "Recycling of strange sets: II. Applications," *Nonlinearity*, vol. 3, p. 361, 1990.

[4] Beyn, W.-J. and Thümmler, V., "Freezing solutions of equivariant evolution equations," *SIAM J. Appl. Dyn. Syst.*, vol. 3, pp. 85–116, 2004.

[5] Birkhoff, G. D., "Proof of the ergodic theorem," *Proc. Natl. Acad. Sci. USA*, vol. 17, no. 12, pp. 656–660, 1931.

[6] Bowen, R., *Equilibrium States and the Ergodic Theory of Anosov Diffeomorphisms*. Berlin: Springer, 1975.

[7] Budanur, N. B., Borrero-Echeverry, D., and Cvitanović, P., "Periodic orbit analysis of a system with continuous symmetry - a tutorial," *Chaos*, vol. 25, no. 7, 2015. arXiv:1411.3303.

[8] Budanur, N. B., Cvitanović, P., Davidchack, R. L., and Siminos, E., "Reduction of the SO(2) symmetry for spatially extended dynamical systems," *Phys. Rev. Lett.*, vol. 114, p. 084102, 2015. arXiv:1405.1096.

[9] Cartan, E., *La méthode du repère mobile, la théorie des groupes continus, et les espaces généralisés*, vol. 5 of *Exposés de Géométrie*. Paris: Hermann, 1935.

[10] Cushman, R. H. and Bates, L. M., *Global Aspects of Classical Integrable Systems*. Boston: Birkhäuser, 1997.

[11] Cvitanović, P., "Invariant measurement of strange sets in terms of cycles," *Phys. Rev. Lett.*, vol. 61, p. 2729, 1988.

[12] Cvitanović, P., Artuso, R., Mainieri, R., Tanner, G., and Vattay, G., *Chaos: Classical and Quantum*. Copenhagen: Niels Bohr Inst., 2014. ChaosBook.org.

[13] Cvitanović, P., Davidchack, R. L., and Siminos, E., "On the state space geometry of the Kuramoto-Sivashinsky flow in a periodic domain," *SIAM J. Appl. Dyn. Syst.*, vol. 9, pp. 1–33, 2010. arXiv:0709.2944.

[14] Cvitanović, P., Gaspard, P., and Schreiber, T., "Investigation of the Lorentz gas in terms of periodic orbits," *Chaos*, vol. 2, pp. 85–90, 1992.

[15] Dangelmayr, G., "Steady-state mode interactions in the presence of 0(2)-symmetry," *Dyn. Sys.*, vol. 1, pp. 159–185, 1986.

[16] Ding, X. and Cvitanović, P., "Periodic eigendecomposition and its application in Kuramoto-Sivashinsky system." arXiv:1406.4885, 2014.

[17] Ezra, G. S., Richter, K., Tanner, G., and Wintgen, D., "Semiclassical cycle expansion for the helium atom," *J. Phys. B*, vol. 24, pp. L413–L420, 1991.

[18] Faisst, H. and Eckhardt, B., "Traveling waves in pipe flow," *Phys. Rev. Lett.*, vol. 91, p. 224502, 2003.

[19] Field, M., "Equivariant dynamical systems," *Bull. Amer. Math. Soc.*, vol. 76, pp. 1314–1318, 1970.

[20] Field, M. J., "Equivariant dynamical systems," *Trans. Amer. Math. Soc.*, vol. 259, no. 1, pp. 185–205, 1980.

[21] Froehlich, S. and Cvitanović, P., "Reduction of continuous symmetries of chaotic flows by the method of slices," *Commun. Nonlinear Sci. Numer. Simul.*, vol. 17, pp. 2074–2084, 2012. arXiv:1101.3037.

[22] Gibson, J. F., Halcrow, J., and Cvitanović, P., "Visualizing the geometry of state-space in plane Couette flow," *J. Fluid Mech.*, vol. 611, pp. 107–130, 2008. arXiv:0705.3957.

[23] Gutzwiller, M. C., "Phase-integral approximation in momentum space and the bound states of an atom," *J. Math. Phys.*, vol. 8, pp. 1979–2000, 1967.

[24] Gutzwiller, M. C., "Phase-integral approximation in momentum space and the bound states of an atom. II," *J. Math. Phys.*, vol. 10, pp. 1004–1021, 1969.

[25] Hopf, E., "A mathematical example displaying features of turbulence," *Commun. Appl. Math.*, vol. 1, pp. 303–322, 1948.

[26] Huygens, C., *L'Horloge à Pendule*. Amsterdam: Swets & Zeitlinger, 1673.

[27] Jones, C. A. and Proctor, M. R. E., "Strong spatial resonance and travelling waves in Benard convection," *Phys. Lett. A*, vol. 121, pp. 224–228, 1987.

[28] Kawahara, G. and Kida, S., "Periodic motion embedded in plane Couette turbulence: Regeneration cycle and burst," *J. Fluid Mech.*, vol. 449, pp. 291–300, 2001.

[29] Krupa, M., "Bifurcations of relative equilibria," *SIAM J. Math. Anal.*, vol. 21, pp. 1453–1486, 1990.

[30] Marqués, F., "On boundary conditions for velocity potentials in confined flows: Application to couette flow," *Phys. Fluids A*, vol. 2, no. 5, pp. 729–737, 1990.

[31] Nagata, M., "Three-dimensional finite-amplitude solutions in plane Couette flow: bifurcation from infinity," *J. Fluid Mech.*, vol. 217, pp. 519–527, 1990.

[32] Nagata, M., "Three-dimensional traveling-wave solutions in plane Couette flow," *Phys. Rev. E*, vol. 55, pp. 2023–2025, 1997.

[33] Poincaré, H., "Sur les solutions périodiques et le principe de moindre action," *C. R. Acad. Sci. Paris*, vol. 123, pp. 915–918, 1896.

[34] Porter, J. and Knobloch, E., "Dynamics in the 1:2 spatial resonance with broken reflection symmetry," *Physica D*, vol. 201, pp. 318 – 344, 2005.

[35] Rowley, C. W. and Marsden, J. E., "Reconstruction equations and the Karhunen-Loéve expansion for systems with symmetry," *Physica D*, vol. 142, pp. 1–19, 2000.

[36] Ruelle, D., "Bifurcations in presence of a symmetry group," *Arch. Rational Mech. Anal.*, vol. 51, pp. 136–152, 1973.

[37] Ruelle, D., *Statistical Mechanics, Thermodynamic Formalism*. Reading, MA: Wesley, 1978.

[38] Rugh, H. H., "The correlation spectrum for hyperbolic analytic maps," *Nonlinearity*, vol. 5, p. 1237, 1992.

[39] Sinai, Y. G., "Gibbs measures in ergodic theory," *Uspekhi Mat. Nauk*, vol. 166, p. 21, 1972.

[40] Sivashinsky, G. I., "Nonlinear analysis of hydrodynamical instability in laminar flames - I. Derivation of basic equations," *Acta Astronaut.*, vol. 4, pp. 1177–1206, 1977.

[41] Smale, S., "Differentiable dynamical systems," *Bull. Amer. Math. Soc.*, vol. 73, pp. 747–817, 1967.

[42] Smale, S., "Topology and mechanics, I.," *Invent. Math.*, vol. 10, pp. 305–331, 1970.

[43] Viswanath, D., "Recurrent motions within plane Couette turbulence," *J. Fluid Mech.*, vol. 580, pp. 339–358, 2007. arXiv:physics/0604062.

[44] Wedin, H. and Kerswell, R. R., "Exact coherent structures in pipe flow," *J. Fluid Mech.*, vol. 508, pp. 333–371, 2004.

[45] Willis, A. P., Cvitanović, P., and Avila, M., "Revealing the state space of turbulent pipe flow by symmetry reduction," *J. Fluid Mech.*, vol. 721, pp. 514–540, 2013. arXiv:1203.3701.

[46] Willis, A. P. and Kerswell, R. R., "Turbulent dynamics of pipe flow captured in a reduced model: puff relaminarisation and localised 'edge' states," *J. Fluid Mech.*, vol. 619, pp. 213–233, 2009.

[47] Willis, A. P., Short, K. Y., and Cvitanović, P., "Relative periodic orbits form the backbone of turbulent pipe flow." arXiv:1504.05825, 2015.

[48] Wintgen, D., Richter, K., and Tanner, G., "The semiclassical helium atom," *Chaos: An Interdisciplinary Journal of Nonlinear Science*, vol. 2, no. 1, pp. 19–33, 1992.

[49] Yoder, J. G., *Unrolling Time: Christiaan Huygens and the Mathematization of Nature*. Cambridge: Cambridge Univ. Press, 1988.